Enhancing gearbox vibration signals under time-varying operating conditions by combining a whitening procedure and a synchronous processing method

Stephan Schmidt[a,*], Radoslaw Zimroz[b], P. Stephan Heyns[a]

[a] *Centre for Asset Integrity Management, Department of Mechanical and Aeronautical Engineering, University of Pretoria, Pretoria, South Africa*
[b] *Faculty of Geoengineering, Mining and Geology, Department of Mining and Geology, Wroclaw University of Science and Technology,Wroclaw, Poland*

Abstract

Condition monitoring is very important to avoid unexpected breakdowns of expensive rotating machines found in the power generation and mining industries. The fault information in vibration signals is often buried in low energy frequency bands. In addition to this, time-varying operating conditions and the presence of impulsive noise results in the signal to have time-varying spectral content, which impedes the condition inference process. The instantaneous power spectrum is a powerful method that can be used for bearing and gear damage detection under time-varying operating conditions. In this work, we propose a new method of using the instantaneous power spectrum for improved fault diagnosis under time-varying conditions by enhancing the fault information in the vibration signals. It is shown on experimental datasets that the proposed method enhances the fault information in the signal, whereafter it can be used to obtain reliable condition indicators under time-varying operating conditions.

Keywords:
Gearbox diagnostics, Whitening, Time-varying operating conditions, Synchronous Geometric Average, Instantaneous Power Spectrum

1. Introduction

Vibration-based condition monitoring is very popular for drive train and bearing monitoring, since the vibration data are rich with fault information [1–3]. Damaged mechanical components result in the signal to contain periodic transients [4, 5]. Therefore, the vibration signals can be analysed to detect the presence of damaged components, determine which component is damaged

*Corresponding author.
Email address: stephan.schmidt@up.ac.za (Stephan Schmidt)

and perform fault trending (i.e. determining changes in the condition of the machine) [3, 6, 7]. However, the vibrations of the rotating machines are not only affected by the instantaneous condition of the machine components, but also the operating conditions (e.g. load, speed, temperature) during the data acquisition process [8, 9]. The ambiguity that results from the fact that changes in the vibration data could be ascribed to both changes in operating condition and changes in machine condition, impedes the reliability of many conventional condition monitoring methods in the power generation (e.g. wind turbines) and the mining (e.g. bucket wheel excavators) industries [8–10].

It is possible to extract the salient fault information from the vibration signal by utilising frequency band identification methods [11–16]. Frequency band identification methods highlight informative frequency bands in the signal and can be used to design a bandpass or matching filter [17–19]. Subsequently, this filter is applied to the measured signal, which is analysed for symptoms of damage [18, 20]. The kurtogram [12], the infogram and related methods [4, 21, 22], the ICS2gram [18], the IFBI$_\alpha$gram [23] and the accugram [24] are examples of frequency band identification methods. After the application of frequency band identification methods, it is necessary to use signal analysis methods such as the Squared Envelope Spectrum (SES) on the filtered vibration signals [25]. However, even though some of the methods are capable of extracting the fault information under time-varying operating conditions, the filtered vibration signals may still contain operating condition information, which makes it difficult to distinguish between changes in the machine and the operating conditions [9].

It is possible to obtain more robust representations of the condition of the machine by comparing the condition indicators against the operating condition information [8, 10], by attenuating the amplitude modulation attributed to varying operating conditions [9], and by identifying the operating condition state in the machine and using this information to segment the machine condition features in quasi-stationary states [26].

Deterministic signal components and dominant frequency bands could impede the detection of damage components [25, 27–29]. Cepstral methods [27]; deterministic-random separation by subtracting the generalised synchronous average [25, 29]; and cepstrum pre-whitening [28] have been used to enhance the fault information or to improve the diagnosability of the damage.

Damaged rotating machine components often result in the instantaneous power of the signal to become more periodic in narrow frequency bands [6, 30, 31]. This makes time-frequency methods well-suited for representing the non-stationary components associated with damaged mechanical components [32–34]. The instantaneous power spectrum of the vibration signal vi-

sualises changes in the instantaneous power of specific frequency bands and is well-suited for rotating machine fault diagnosis [6, 35, 36]. However, it could be difficult to detect incipient damage from the two-dimensional representation and therefore further processing is necessary. Antoni and Hanson [37] used the cyclic spectrum of the instantaneous power spectrum, referred to as the cyclic modulation spectrum, for ship surface detection. Abboud and Antoni [38] extended the cyclic modulation spectrum for fault detection under time-varying operating conditions. Urbanek et al. [36] proposed the synchronous average of the instantaneous power spectrum for detecting bearing damage and showed that it is very effective for wind turbine bearing fault diagnosis under time-varying operating conditions.

The instantaneous power spectrum is rich with fault and operating condition information, however, it is difficult to detect the damage components when there are frequency bands with high energy levels. This is illustrated in Figure 1 for the vibration signals acquired from a healthy gearbox and a gearbox with a damaged gear. The spectrograms in Figures 1(a) and (b) are dominated by frequency bands without much fault information. This makes it difficult to detect the fault information in the frequency range of 350 to 700 Hz in Figures 1(b) and (c). The

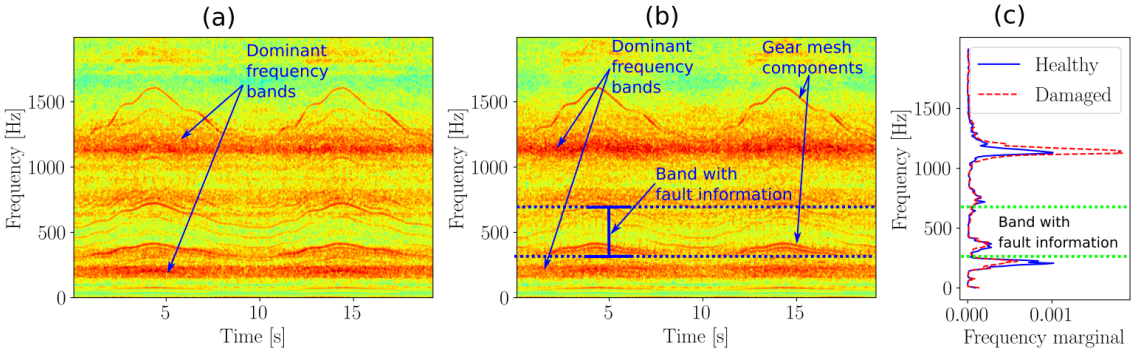

Figure 1: The spectrograms of a vibration signal acquired from a healthy gearbox and a damaged gearbox are presented in (a) and (b) respectively. The corresponding frequency marginals, i.e. integrating the spectrograms over time, are presented in (c). The vibration signals were acquired from the experimental test-rig presented in Section 3.

damage would be easier to detect if the dominant frequency bands without fault information were attenuated. After the dominant frequency bands are attenuated, the time-frequency distribution needs to be processed to ensure that the damage can be detected.

Hence, in this work, we propose a new method to process the instantaneous power spectrum for fault diagnosis under time-varying and non-Gaussian noise conditions. Firstly, the angle-frequency instantaneous power spectrum is whitened, whereafter the signal is processed to remove

spurious signal components attributed to impulsive components. This ensures that weak fault components are amplified and a reliable representation is obtained for fault diagnosis under time-varying and in the presence of non-fault related impulsive components. In summary, this method has the following benefits:

- It is very simple to implement and only requires the availability of a vibration measurement, an estimate of the instantaneous phase of the shafts of the rotating machine, and the fault orders of the rotating machine.
- It performs very well on data acquired under time-varying operating and in the presence of cyclostationary components that are not related to the component-of-interest.

The layout of this paper is as follows: In Section 2, the proposed method is presented, whereafter it is investigated in Section 3 on two experimental datasets that were acquired under time-varying operating conditions. Finally, the work is concluded in Section 4. Appendix A provides additional information pertaining to the proposed method and Appendix B contains an overview of a synthetic signal used for the illustrations in this paper.

2. Proposed method

The process diagram of the proposed method is presented in Figure 2. Firstly, the Instantaneous Power Spectrum (IPS) of the measured vibration signal is calculated, whereafter a whitening function is estimated and used to normalise the different frequency bands of the IPS. Thereafter, the whitened IPS is processed using a synchronous processing procedure (e.g. Synchronous Average [36]) and the processed IPS is integrated over all frequency bands. This representation is subsequently used for fault diagnosis (e.g. fault detection, fault identification and fault trending). Our contribution in this work is specifically in the whitening and the syn-

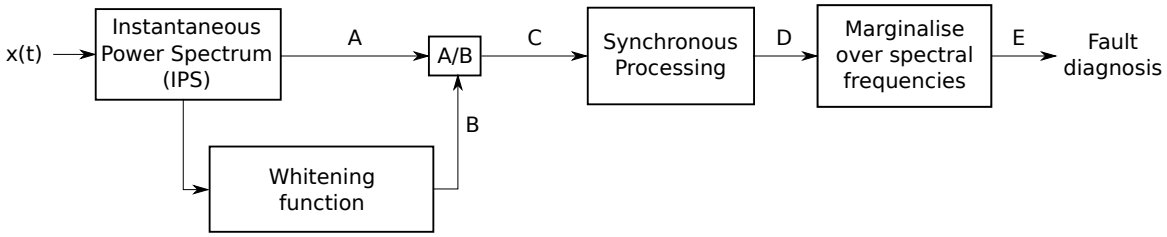

Figure 2: Process diagram of the proposed method. A: Instantaneous Power Spectrum (IPS); B: Whitening function; C: The whitened IPS obtained by dividing the IPS by the whitening function; D: The processed whitened IPS; E: The integrated IPS which is used for fault diagnosis.

chronous processing steps.

Each step in Figure 2 is discussed in detail in the subsequent sections.

2.1. Instantaneous Power Spectrum (IPS)

The Time-Frequency Instantaneous Power Spectrum (TF-IPS) of a discrete-time vibration signal $\boldsymbol{x} = [x[0], \ldots, x[N-1]]$, sampled with a frequency f_s, is given by [38]:

$$I_{xx}\left(t_n, f_m; \Delta f\right) = \frac{1}{N \cdot f_s \cdot ||h||^2} \cdot \left|X\left(t_n, f_m; \Delta f\right)\right|^2, \tag{1}$$

where $X\left(t_n, f_m; \Delta f\right)$ denotes the Short-Time Fourier Transform (STFT) of the signal x, Δf is the spectral frequency resolution of the STFT, N is the length of the signal, h is a windowing function such as a Hamming window, the absolute time at time step n is given by $t = t_n/f_s$ and the spectral frequency associated with the mth bin is denoted f_m.

The TF-IPS is ill-suited for application under time-varying operating conditions, due to the fact that the signal components are periodic in the angle domain [36, 38]. In contrast, the impulses generated by damaged mechanical components usually excite time-invariant carriers and therefore the spectral frequency bands are not dependent on the speed. Urbanek et al. [36] and Abboud et al. [39] proposed that signals from damaged components such as bearings should be described in an angle-frequency representation and therefore the Angle-Frequency IPS (AF-IPS), obtained with [36, 38]

$$I_{xx}\left(\varphi_a, f_m; \Delta f\right) = \underset{t \to \varphi}{\mathrm{OT}}\left\{I_{xx}\left(t_n, f_m; \Delta f\right)\right\}, \tag{2}$$

should be used instead of the TF-IPS for condition monitoring under time-varying operating conditions. The Order Tracking (OT) operator, converts the time domain variable t_n to an angle domain variable φ_a, with this operation performed separately for each frequency band in the TF-IPS [36, 38]. If the rotational speed is unavailable, tacholess order tracking methods can be used to estimate the rotational speed from the vibration signal [40, 41].

2.2. Whitening function

It is desired to attenuate the dominant spectral frequency bands in the AF-IPS to ensure that the fault information is enhanced. The whitened IPS refers to the IPS with its dominant frequency bands attenuated. We use a whitening function, denoted $W(f)$, to obtain the whitened IPS as follows:

$$I_w\left(\varphi_a, f_m; \Delta f\right) = \frac{I_{xx}\left(\varphi_a, f_m; \Delta f\right)}{W(f_m)}. \tag{3}$$

This whitening function should attenuate the transfer function effects as the signal travels from the source (e.g. impact) to the sensors as well as other stationary components, without attenuating the cyclostationary fault information in the signal.

The angle-average of the AF-IPS, i.e. $\left\langle I_{xx}(\varphi_a, f_m)\right\rangle_a$, which is related to Welch's estimate of the power spectral density of the signal x, can be used to obtain an estimate of the whitening function

$$\hat{W}^{avg}(f_m) = \left\langle I_{xx}(\varphi_a, f_m)\right\rangle_a. \tag{4}$$

The arithmetic average over the a index is denoted $\left\langle \cdot \right\rangle_a$ in Equation (4). This function is used in the calculation of the Cyclic Modulation Coherence (CMC) [37]. However, in Ref. [42] it is the shown that the power spectral density contains fault information as well. Furthermore, in Appendix A it is shown that Equation (4) is dependent on the magnitude of the damage components. This indicates that the estimator given by Equation (4) would overestimate the actual whitening function $W(f_m)$ if damage is present and this estimation error changes as the magnitude of the damage components changes. This would result in the fault information to be attenuated, with the amount of attenuation being dependent on the magnitude of the signal components.

Damage often manifests as sparse components in the instantaneous power spectrum and the cyclic spectrum [35, 36]. Hence, a more reliable estimate of the whitening function would be obtained by using the geometric angle-average of the instantaneous power spectrum instead of the angle-average. The Geometric angle-Average Whitening (GAW) function can be written as

$$\hat{W}^{geo}(f_m) = \exp\left(\left\langle \log\left(I_{xx}(\varphi_a, f_m)\right)\right\rangle_a\right), \tag{5}$$

which emphasises that the average of the logarithm of the IPS is calculated as opposed to the average of the IPS in Equation (4). It is expected that damaged mechanical components would result in the tails of the distribution of the IPS to increase. Smith et al. [18] proved that the average of a logarithm of a function converges better for long-tailed distributions than using the average of the function. Hence, Equation (5) is expected to be a more appropriate estimate of the whitening function. This is demonstrated on a synthetic signal in Appendix B.

2.3. Synchronous Processing of the Instantaneous Power Spectrum

The whitening function in Equation (5) would only ensure that noise levels in the frequency bands of the IPS are the same. Additional processing is necessary to perform fault diagnosis with the whitened AF-IPS. Urbanek et al. [36] used the Synchronous Average of the IPS (SA-IPS)

to highlight the impulses attributed to a damaged wind turbine bearing. The SA-IPS can be calculated as follows for the whitened IPS:

$$\bar{I}_w^{avg}(\varphi_i, f_m; \Phi_0) = \frac{1}{K} \sum_{k=0}^{K-1} I_w(\varphi_i + k \cdot \Phi_0, f_m), \tag{6}$$

with Φ_0 being the cyclic period (i.e. reciprocal of the cyclic order) of the component of interest, K is the number of cycles, and $0 \leq \varphi_i < \Phi_0$. The SA procedure provides an estimate with less variance and is easier to interrogate than the full IPS and should therefore be preferred over the raw instantaneous power spectrum for fault diagnosis.

Since the instantaneous power spectrum reflects the instantaneous changes in the signal, it would also be sensitive to impulsive components that are not associated with the machine component under consideration. This is expected for machines operating in impulsive environments and when the non-synchronous components are damaged [31, 43, 44]. Hence, we propose that the Synchronous Geometric Average (SGA) of the whitened IPS

$$\bar{I}_w^{geo}(\varphi_i, f_m; \Phi_0) = \exp\left(\frac{1}{K} \sum_{k=0}^{K-1} \log\left(I_w\left(\varphi_i + k \cdot \Phi_0, f_m\right)\right)\right), \tag{7}$$

should be used instead of the SA-IPS for signals acquired from impulsive environments, or if the non-synchronous components are damaged. This is attributed to the fact that the geometric average is much more robust to outliers than the arithmetic average. The synchronous geometric average is used in the calculation of the correlated kurtosis [45]. The correlated kurtosis is used as an important step to deconvolve a signal for diagnosing rotating machines [46, 47].

2.4. Fault trending

Even though the representation given by Equation (7) could be very effective for fault detection, it is desired to obtain a single indicator that can be used for fault trending. The root-mean-square of the vibration signal is one of the most popular indicators for prognosis [48], however, it does not allow the condition of specific components in the gearbox to be inferred. It is therefore necessary to use a targeted feature (e.g. degree-of-cyclostationarity) to ensure that we can infer the condition of specific mechanical components [18, 49].

In this work, we use the spectral negentropy [4] of the synchronous average of the processed instantaneous power for fault trending. This is calculated as follows. Firstly, the instantaneous power associated with the synchronous geometric average of the instantaneous power spectrum is calculated by marginalising over the spectral frequency variable

$$e_w^{geo}(\varphi_i; \Phi_0) = \frac{1}{M} \sum_{m=0}^{M-1} \bar{I}_w^{geo}(\varphi_i, f_m; \Phi_0), \tag{8}$$

with Φ_0 being the cyclic order of the component-of-interest. Equation (8) is referred to as the integrated IPS in this work and is defined in the domain $0 \leq \varphi_i < \Phi_0$. Secondly, the spectral negentropy of the integrated IPS [4]

$$z_w(\Phi_0) = \left\langle \frac{e_w^{geo}(\varphi_i;\Phi_0)}{\left\langle e_w^{geo}(\varphi_n;\Phi_0)\right\rangle_n} \cdot \log\left(\frac{e_w^{geo}(\varphi_i;\Phi_0)}{\left\langle e_w^{geo}(\varphi_n;\Phi_0)\right\rangle_n} \right) \right\rangle_n , \tag{9}$$

is calculated to obtain the condition indicator corresponding to the component with a cyclic period Φ_0. The condition indicator $z_w(\Phi_0)$ can be used to monitor the condition of specific mechanical components (e.g. to distinguish between a gear and a bearing fault) with the additional benefit that it is very simple to implement.

2.5. Summary of method

The calculation procedure of the proposed method is presented in Figure 3 on synthetic vibration data presented in Appendix B. In this signal, a damaged machine component is simulated by generating an impulse at 180 degrees of the shaft, which repeats with each shaft rotation. The impulses are hidden by the two dominant spectral frequency bands at 1000 and 2000 Hz seen in Figure 3(a). In the proposed method, the whitening function, shown in Figure 3(b), is used to whiten the IPS before the SGA is calculated. It is clear from this result in Figure 3(c) that the GAW attenuates the dominant frequency bands and the SGA in Figure 3(d) is able to effectively extract the periodic impulses. This results in an intuitive integrated IPS with the damaged component clearly seen in Figure 3(e). This result is compared to the case where only SGA is performed on the raw IPS (i.e. steps 3(a), 3(f) and 3(g)). Even though the SGA is used, it is not possible to detect the damage in Figure 3(g) without the whitening procedure.

In the next section, the proposed method is investigated on experimental data that were acquired under time-varying operating conditions and compared to various other IPS processing methods as outlined in Table 1.

3. Experimental investigation

In this section, the proposed method is investigated on experimental data that were acquired under time-varying operating conditions. Firstly, an overview of the experimental test-rig is presented in Section 3.1, whereafter a localised gear damage dataset is considered in Section 3.2 and a distributed gear damage dataset is considered in Section 3.3. The localised gear damage dataset highlights the suitability of the proposed method to attenuate impulsive components

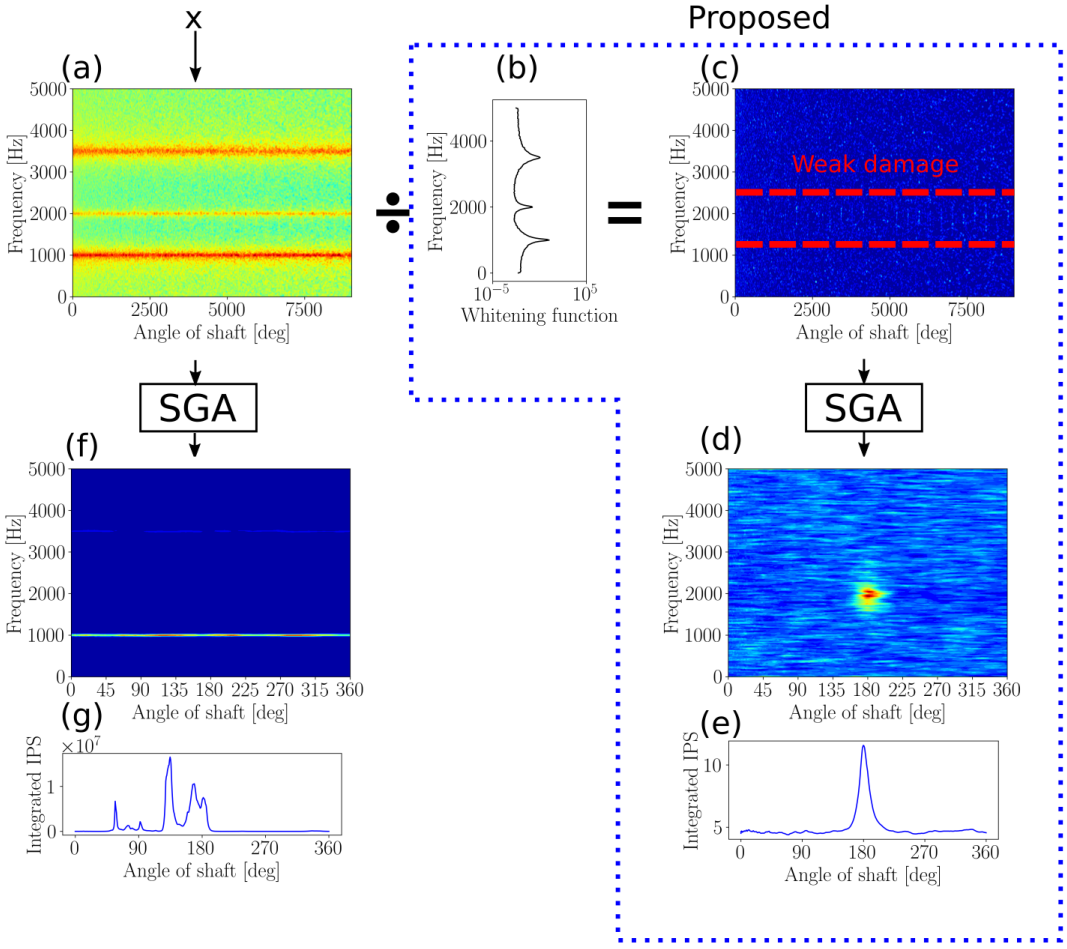

Figure 3: The illustrated process diagram of the proposed method. (a) Angle-Frequency Instantaneous Power Spectrum (AF-IPS); (b) Geometric Average Whitening (GAW) function; (c) Geometric Average Whitened IPS (GAW-IPS); (d) Synchronous Geometric Average of the GAW-IPS (SGA-GAW-IPS); (e) Integrated SGA-GAW-IPS; (f) Synchronous Geometric Average IPS (SGA-IPS); (g) Integrated SGA-IPS.

Table 1: The different methods which are compared in this work. The whitening column indicates the whitening procedure (e.g. Average Whitening (AW), Geometric Average Whitening (GAW)) that is performed on the IPS and the synchronous processing column indicates the synchronous processing (e.g. Synchronous Average (SA) or Synchronous Geometric Average (SGA)) that is performed.

Abbreviation	Whitening	Synchronous Processing	Additional remarks
SA-IPS	None	SA	Used in Ref. [36]
SGA-IPS	None	SGA	
SGA-AW-IPS	AW	SGA	
SGA-GAW-IPS	GAW	SGA	Proposed method

unrelated to the component-of-interest and the distributed gear damaged dataset highlights the suitability of the method to attenuate time-varying operating conditions.

3.1. Experimental test-rig

The experimental test-rig presented in Figure 4 is located in the Centre for Asset Integrity Management (C-AIM) laboratory of the University of Pretoria. The test-rig in Figure 4(a)

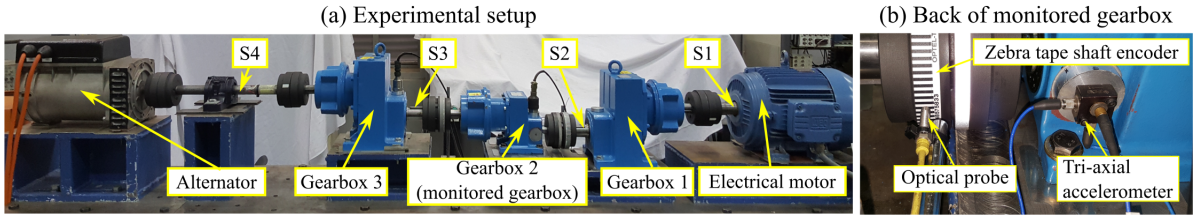

Figure 4: The experimental test-rig that was used to generate the data is shown in (a), with the back of the monitored gearbox presented in (b). The different shafts of the test-rig are denoted by S1, S2, S3, and S4.

consists of an alternator, an electric motor and three industrial helical gearboxes. The electric motor, which drives the system, and the alternator, which dissipates the rotational energy, are separately controlled using a personal computer. The first gearbox (i.e. Gearbox 1) reduces the rotational speed of the motor with a factor of 4.93, with the centre gearbox (i.e. Gearbox 2) and the last gearbox (i.e. Gearbox 3) increasing the input speed with a factor of 1.85 and 4.93 respectively. Gearbox 2 is a parallel shaft helical gearbox that consists of a gear and pinion, with its rotational speed being estimated with an optical probe and a zebra tape shaft encoder located at its input shaft. The zebra tape shaft encoder and the optical encoder are presented in Figure 4(b) and sampled at 51.2 kHz. Since the gear of Gearbox 1 is connected to the reference

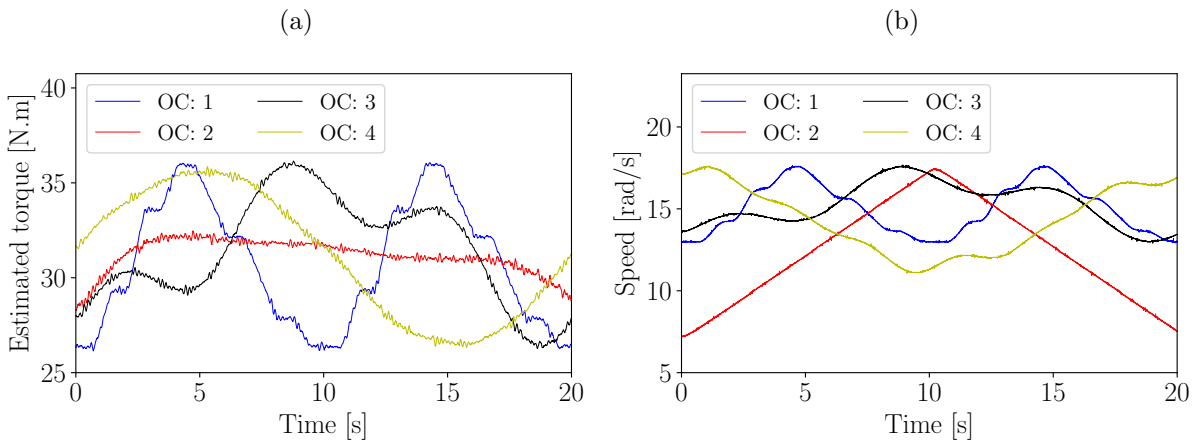

Figure 5: The operating conditions that were present at the input shaft (i.e. S2 in Figure 4) of the monitored gearbox.

shaft, it rotates at 1.0 orders of the input shaft, while the pinion rotates at 1.85 orders of the input shaft. This means that the cyclic period of the gear is $\Phi_0 = 1.0$ rotations and the cyclic period of the pinion is $\Phi_0 = 0.54054$ rotations.

The axial component of the tri-axial accelerometer, located on the back of the monitored gearbox and shown in Figure 4(b), is used for monitoring the condition of the components of Gearbox 2. The acceleration signal is sampled at 25.6 kHz. We found that the vibration data acquired from the monitored gearbox contain much impulsive information irrespective of the condition of the gears. This is attributed to the contact made between a floating bearing and the casing of the gearbox when axial loads are applied on the shaft. The impulsive noise and the fact that helical gears are used, impede the application of many conventional signal analysis techniques.

The vibration data were acquired under different time-varying operating condition profiles, with the four operating conditions considered in this work presented in Figure 5. These operating conditions ensure that we can evaluate the suitability of the proposed method for applications where the load and speed of the machine vary over time.

Two different gear conditions are investigated in the monitored gearbox (i.e. Gearbox 2 in Figure 4). In the first experiment, localised gear damage was induced in the gear and in the second experiment, distributed gear damage was induced. In both of the aforementioned cases the pinion was in a healthy condition. In the next section, the localised gear damage results are presented.

(a) Before (b) After

Figure 6: The gear that was used in the localised gear damage experiment. The gear before the fatigue experiment was started is shown in Figure 6(a) and after the test was completed is shown in Figure 6(b).

3.2. Localised gear damage results

Localised gear damage such as root cracks significantly reduce the life of the gears and therefore need to be detected as early as possible [30, 31]. A slot was seeded in the root of a single gear tooth of Gearbox 2, with the result shown in Figure 6(a). This gear was used in the monitored gearbox with a healthy pinion, whereafter the gearbox was operated with operating condition two (i.e., OC 2 in Figure 5) for approximately 20 days. After the completion of the experiment, the gearbox was missing a tooth, with this gear presented in Figure 6(b). Two-hundred measurements, approximately evenly spaced over the life of the gear (i.e. from the condition shown in Figure 6(a) to the condition shown in Figure 6(b)), are considered in this section. The gear damage in Figure 6(a) is difficult to detect due to the presence of impulsive noise and the fact that helical gears are used in the monitored gearbox.

3.2.1. IPS and the integrated IPS

The proposed procedure (SGA-GAW-IPS) and the additional methods (SA-IPS, SA-AW-IPS, SGA-IPS), described in Table 1, were calculated for each measurement in the localised damaged dataset. Firstly, the SA-IPS, the SA-AW-IPS and the SGA-GAW-IPS are presented in Figure 7 for one of the measurements. The localised gear damage can faintly be seen on the gear in Figure 7(a) in the lower frequency band between 90 and 180 degrees. However, the SA-IPS of the pinion looks very similar to the SA-IPS of the gear and the SA-IPS of the gear contains dominant components in the high-frequency bands, which are spread around the circumference of the gear. These dominant frequency components are attributed to the impulsive signal components, which makes it difficult to correctly infer the condition of the gear and the pinion.

The SA-AW-IPS method was implemented for the same signal investigated in Figure 7(a)

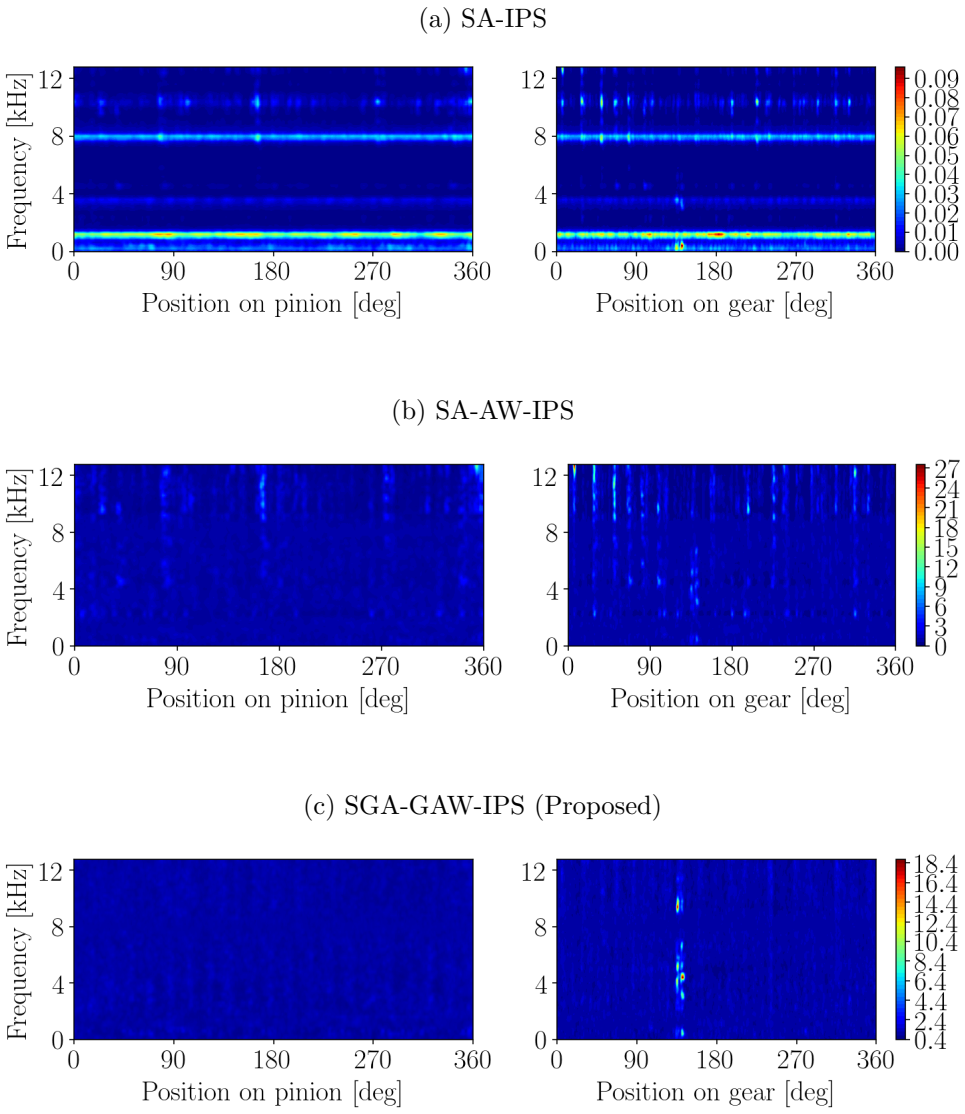

Figure 7: A synchronous representation of the Instantaneous Power Spectrum (IPS) obtained with three different processing methods discussed in Table 1. Abbreviations: Synchronous Average of the IPS (SA-IPS); Synchronous Average of the Averaged Weighted IPS (SA-AW-IPS); Synchronous Geometric Average of the Geometric Average Whitening function of the IPS (SGA-GAW-IPS).

with the results of the gear and the pinion presented in Figure 7(b). It is not possible to see the gear damage in Figure 7(b), because the average whitening procedure attenuates the dominant frequency bands as well as the fault information in the signal.

Lastly, the results for the proposed method (SGA-GAW-IPS) are presented in Figure 7(c). In the proposed method, the geometric averages of the different frequency bands are used to whiten the IPS, whereafter the synchronous geometric average is calculated of the whitened IPS. The synchronous geometric average ensures that non-synchronous impulses are removed from the representation and therefore provides a more reliable representation in the presence of impulsive noise. In Figure 7(c), the gear contains a very dominant component that is localised at approximately 135 degrees, with the rest of the IPS being uniform. The reference point of the shaft position was measured from the butt joint error of the zebra tape shaft encoder, with the 135 degrees being measured from this point. The SGA-GAW-IPS of the pinion is uniform and does not contain any evidence of damage. Hence, the proposed method is capable of providing the correct condition of the gear and the pinion.

Since the instantaneous power spectra will be converted to a scalar metric after integrating over the spectral frequencies, it is important to compare the different integrated IPSs. The integrated SA-IPS, the integrated SA-AW-IPS, and the integrated IPS obtained with the proposed method (SGA-GAW-IPS) are compared in Figure 8 for the same signal investigated in Figure 7. The integrated SA-IPS and the integrated SA-AW-IPS, presented respectively in Figures 8(a) and 8(b), do not indicate the correct condition of the gear and the pinion. This is due to the fact that the SA-IPS contains dominant frequency bands that were also present in the IPS, while the SA-AW-IPS attenuated the fault information in the IPS. In contrast, the integrated IPS obtained with the proposed method, performs much better as seen in Figure 8(c); it is easy to distinguish between the healthy pinion and the damaged gear and the localised gear damage is very prominent at approximately 135 degrees.

Lastly, the integrated SA-IPS and the integrated SGA-GAW-IPS are compared in Figure 9 for all the considered measurements in this dataset. It is clear that the integrated SA-IPS method cannot attenuate the impulsive noise components and therefore makes the damage difficult to detect. It is only possible to see the damage in the SA-IPS because the different measurements were aligned to ensure that the damage on the gear remains at the same position. In contrast, the integrated SGA-GAW-IPS is able to attenuate the impulsive noise components with the damaged gear components clearly seen. This makes the integrated SGA-GAW-IPS a very reliable representation of the condition of the gears.

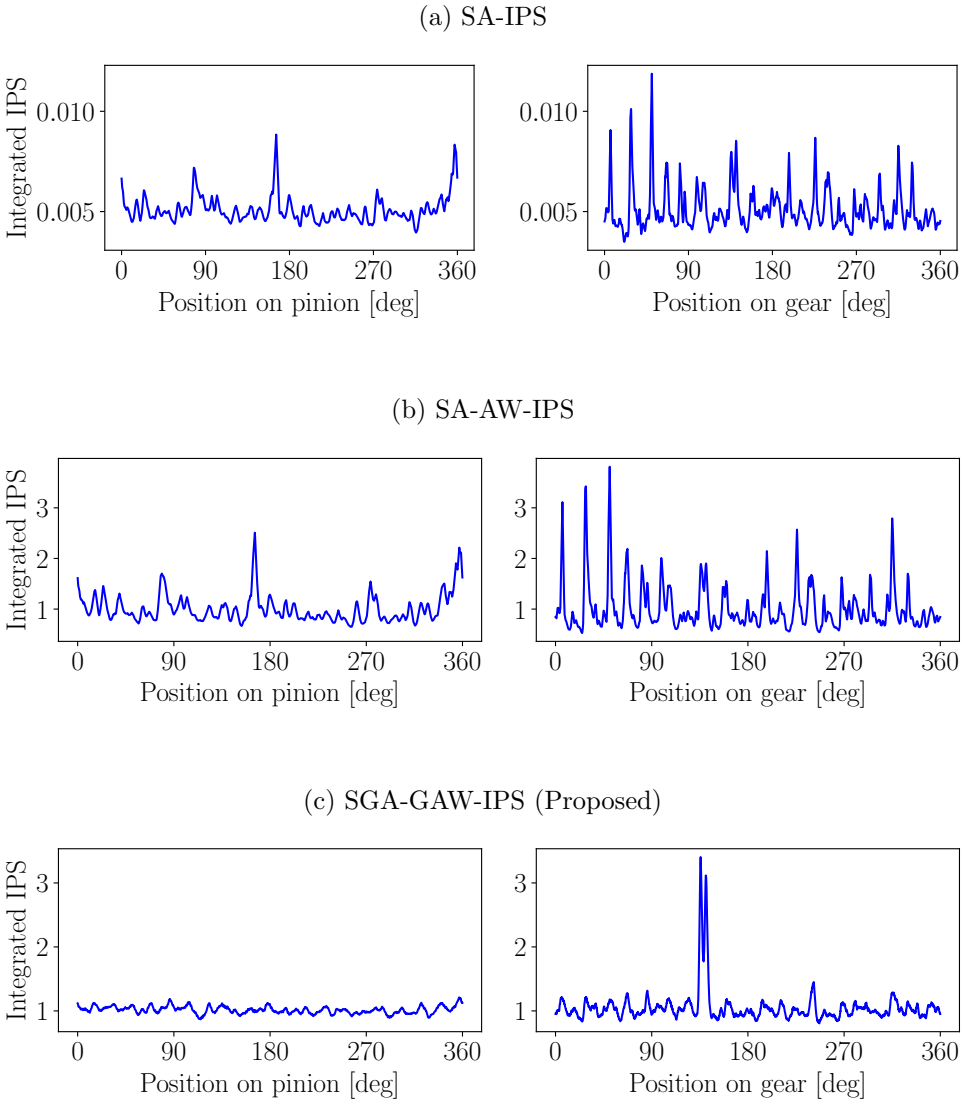

Figure 8: The integrated IPS obtained with three different processing methods for the measurement investigated in Figure 7. Abbreviations: Synchronous Average of the IPS (SA-IPS); Synchronous Average of the Averaged Weighted IPS (SA-AW-IPS); Synchronous Geometric Average of the Geometric Average Whitening function of the IPS (SGA-GAW-IPS).

(a) SA-IPS (b) SGA-GAW-IPS (Proposed)

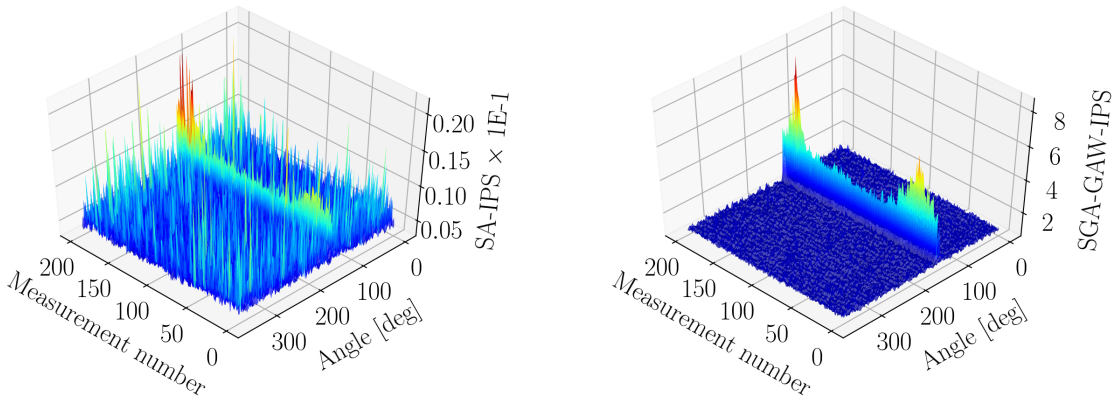

Figure 9: The integrated SA-IPS and the integrated SGA-GAW-IPS are compared for all measurements in the localised gear damage experiment.

3.2.2. Condition indicators

The condition indicators, calculated for the 200 measurements, are presented in Figure 10, for the four methods discussed in Table 1. The condition indicator of the proposed method in Figure 10(a) is extremely sensitive to changes in the condition of the gear component. The damaged gear started with a small slot in the root of the tooth, which ultimately resulted in the tooth to fail. The initial changes of the condition indicator of the gear in Figure 10(a) is attributed to the development of a crack and the final increase of the condition indicator is attributed to the failure of the gear tooth. The slight decrease of this condition indicator at the last few measurements seems to be attributed to the following: The damaged gear tooth impeded the natural meshing of the gear and the pinion in the last few measurements, which increased the vibration levels during meshing. After the gear tooth failed and was removed from meshing, the meshing would become more smooth, which would result in a slight decrease of the vibration levels. This behaviour is also observed in the synchronous representation in Figure 9(b). Since the pinion is in a healthy condition for the duration of the experiment, its condition indicator in Figure 10(a) remains constant with respect to the measurement number.

The condition indicator obtained with the SA-IPS is presented in Figure 10(b). The results contain much more noise, with a change in the gear condition only seen at measurement number 125. The SA-IPS performs much better than expected; it is possible to see a change in the condition of the gear despite its susceptibility to the non-synchronous impulsive components

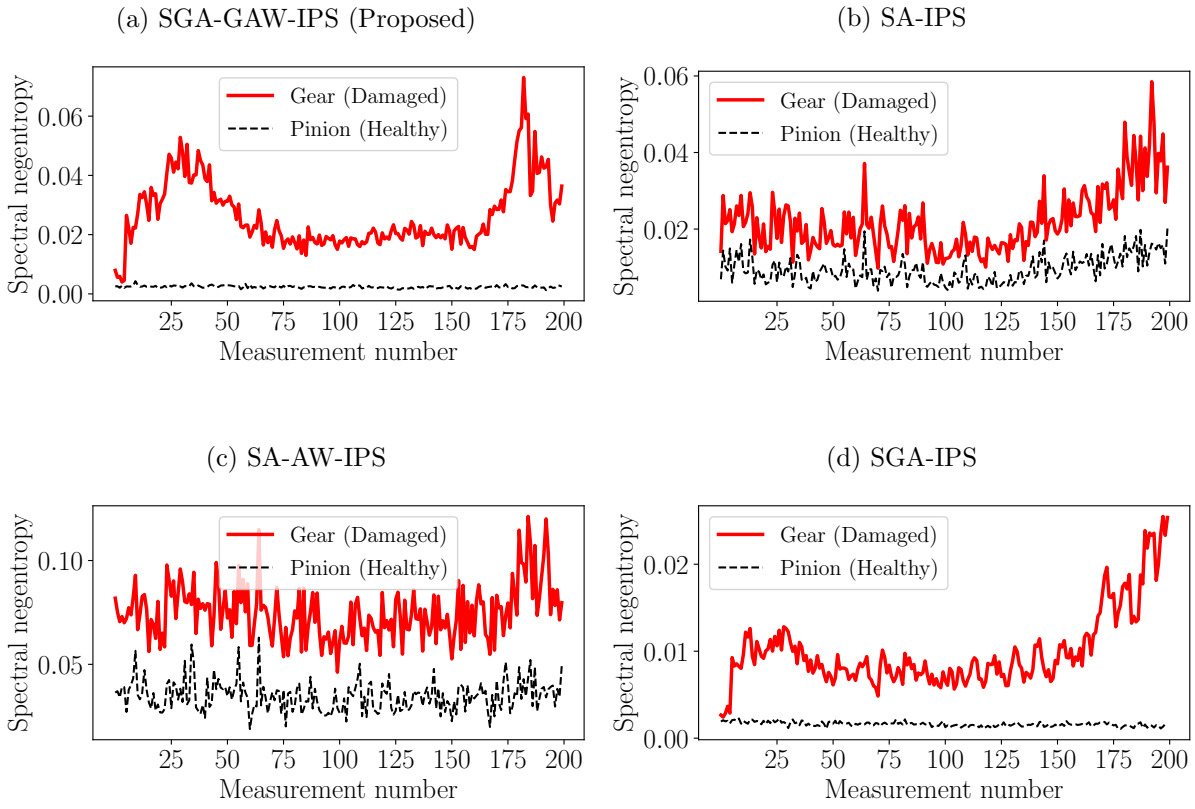

Figure 10: The spectral negentropy of the integrated IPS obtained of the distributed gear damage experiment. The condition indicators of the proposed method, the Synchronous Geometric Average of the Geometric Average Whitened angle-frequency Instantaneous Power Spectrum (SGA-GAW-IPS), the Synchronous Average IPS without performing whitening (SA-IPS), the Synchronous Average of the Average Whitened IPS (GA-AW-IPS) and the Synchronous Geometric Average of the IPS (SGA-IPS) (without performing any whitening procedure) are compared.

seen in Figure 9(a). This is attributed to the fact that these impulsive components remained constant throughout the experiment. However, the condition indicator of the pinion increases over the measurement number even though it was healthy for the duration of the test. This erroneously indicates that both the gear and the pinion are deteriorating over time. This incorrect information is attributed to the fact that the SA-IPS of the pinion is not independent of the non-synchronous damaged components associated with the gear. Therefore, its metrics are not reliable for performing fault trending.

The condition indicator of the SA-AW-IPS in Figure 10(c) performs much worse than the SA-IPS, because it is not even possible to see a change in the condition indicator of the gear. This is attributed to the fact that the whitening function attenuates the fault information and therefore makes the associated integrated IPS and all of its metrics unreliable for fault trending.

Lastly, the condition indicator obtained with the SGA-IPS (i.e. the proposed method without utilising the whitening function) is presented in Figure 10(d). The SGA-IPS performs much better than the SA-IPS, which indicates that the SGA should be preferred to the SA of the IPS. The behaviour of the SGA-IPS in Figure 10(d) is very similar to the proposed method; after the initial increase there is a slight decrease in the condition indicator, whereafter the condition indicator increases again in the final stages of the experiment. However, the SGA-IPS is not as sensitive to changes in the condition of the gear as the proposed SGA-GAW-IPS method.

Since the same operating conditions were present for all measurements in this dataset, it is not possible to evaluate the benefits of using the proposed method for fault trending under time-varying operating conditions. In the next section, the ability of the proposed whitening function (i.e. GAW) to attenuate the varying operating condition information is shown.

3.3. Distributed gear damage results

Distributed gear damage is difficult to detect and can result in more severe damage to develop, which could ultimately result in the gearbox to fail [50]. Distributed gear damage was introduced on the gear of the monitored gearbox by leaving the gear in a corrosive environment for an extended period of time. This damaged gear is shown in Figure 11(a). This gear was operated for eight days whereafter the test was stopped due to excessive vibrations. The excessive vibrations were caused by a large portion of the gear being severely damaged. In Figure 11(b), the gear is presented after the experiment was completed, with the damaged gear portion and the three damaged teeth (i.e. T1, T2, and T3) highlighted. Due to the rotation of the gear, T3 meshes before T2, and T2 meshes before T1. The gearbox was sequentially operated with the operating

(a)

(b)

Figure 11: The gear with distributed gear damage before the experiment started and after the experiment was completed are shown in Figures 11(a) and 11(b) respectively. The three severely damaged gear teeth are labelled T1, T2, and T3 in (b).

conditions shown in Figure 5, i.e. the operating condition sequence was OC $1, 2, 3, 4, 1, 2$ etc. for the duration of the test. In total, 320 measurements were taken during the experiment.

The integrated SA-IPS and the integrated SGA-GAW-IPS are presented in Figure 12 over measurement number.

The damaged portion of the gear is prominent in the region of 0 degrees for both the SA-IPS and the SGA-GAW-IPS. However, the SGA-GAW-IPS in Figure 12(b) is more sensitive to changes in the condition of the gear, with different prominent events, labelled A to G, seen. Since the gearbox was not opened during the tests to preserve the integrity of the experiment, we do not exactly know the physical mechanisms behind the observed events. However, it is possible to speculate by using both the damaged gears in Figure 11 and the results in Figure 12: The initial corroded gear had an uneven surface which would have resulted in high-localised stresses during gear meshing. These localised stresses would increase the surface wear, which would smooth the uneven surface and then decrease the vibration levels. The running-in process of the corroded gear is highlighted by A and B in Figure 12. The events highlighted by C (at measurement 72), D (at measurement 148), E (at measurement 148), F (at measurement 232) and G (at measurement 260) are attributed to the deterioration and failure of the three gear teeth T1, T2 and T3 highlighted in Figure 11. In contrast, only the events at measurement

(a) SA-IPS

(b) SGA-GAW-IPS (Proposed)

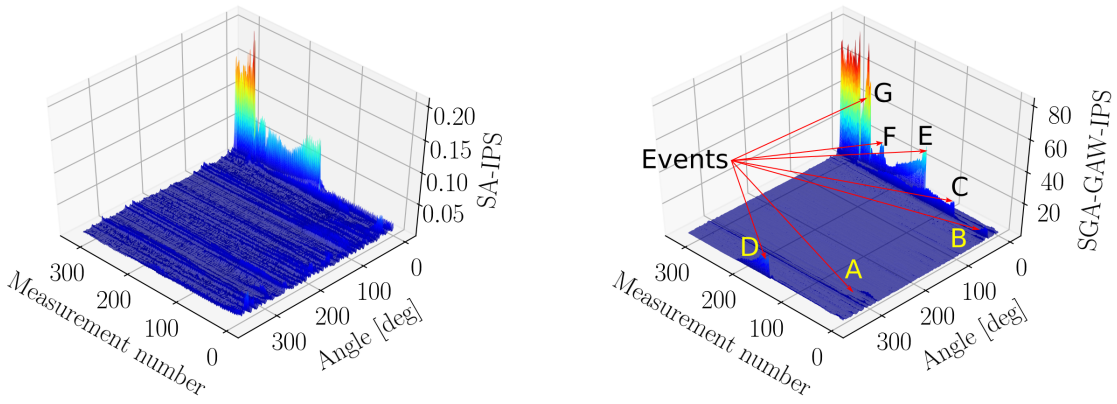

Figure 12: The integrated SA-IPS and the integrated SGA-GAW-IPS are compared for all measurements in the distributed gear damage experiment. In Figure 12(b), different events are highlighted by the arrows and labelled from A to G.

number 148 and 280 are seen in the SA-IPS in Figure 12(a).

The same procedure was performed as for the localised gear damage section to calculate the condition indicators of the SA-IPS, SGA-IPS, SGA-AW-IPS and SGA-GAW-IPS, with the results presented in Figure 13. The condition indicator for the proposed method, presented in Figure 13(a), performs exceptionally well, as it is clearly possible to distinguish between a healthy pinion and a damaged gear and it is sensitive to different events in the signal (e.g. events seen at measurements 72, 148, 232, 260, 280).

The SA of the IPS is also capable of detecting a change in the condition of the gear as shown in Figure 13(b). However, only two events are clearly seen, i.e. at measurement numbers 148 and 280. This indicates that it is less sensitive than the proposed method to changes in the condition of the machine. Additionally, the condition indicator of the pinion also changes over measurement number, which means that it does not accurately convey the condition of the machine components.

The metric associated with the integrated SA-AW-IPS is presented in Figure 13(c) with similar events seen as the SA-IPS metric in Figure 13(b). The condition indicator associated with the SA-AW-IPS contains much more noise, which means that it would be difficult to detect subtle changes in the condition indicator. This noise is attributed to the sensitivity of the average whitening function to the condition of the gear.

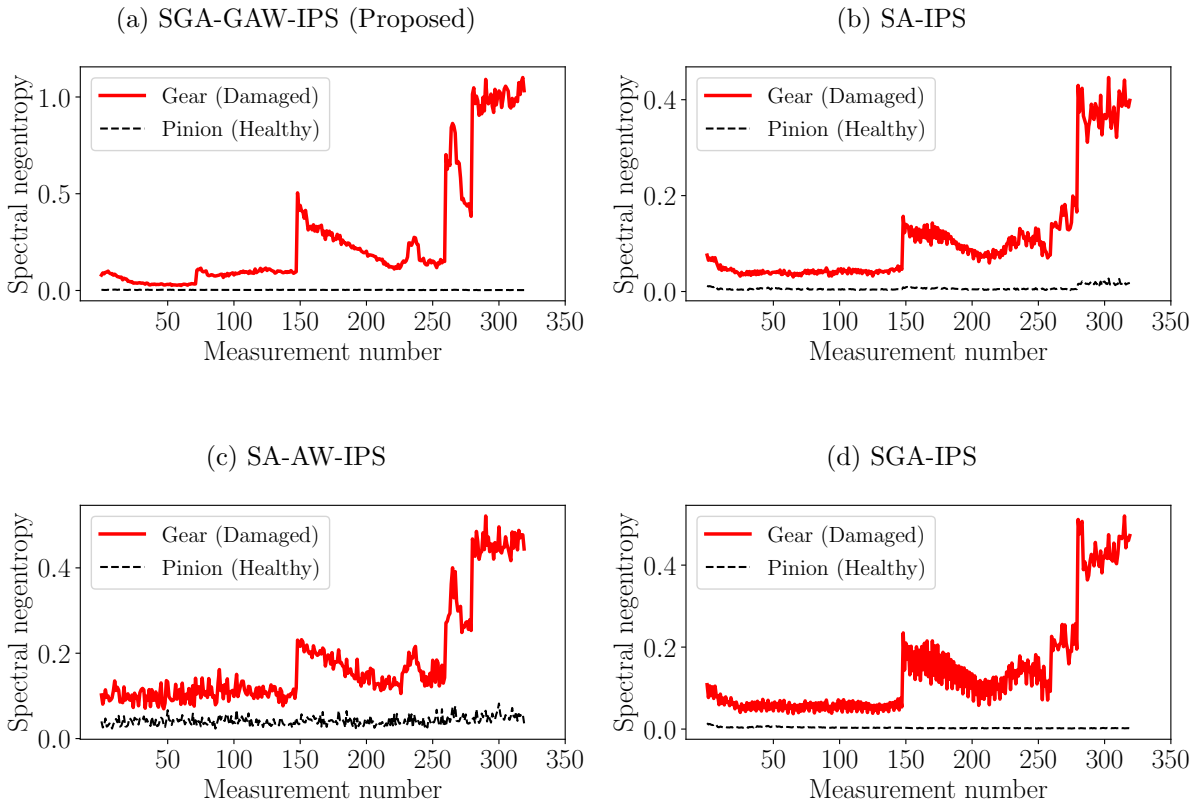

Figure 13: The spectral negentropy of the integrated IPS obtained of the distributed gear damage experiment. The condition indicators of the proposed method, the Synchronous Geometric Average of the Geometric Average Whitened angle-frequency Instantaneous Power Spectrum (SGA-GAW-IPS); the Synchronous Average IPS without performing whitening (SA-IPS); the Synchronous Average of the Average Whitened IPS (GA-AW-IPS); and the Synchronous Geometric Average of the IPS (SGA-IPS) (without performing any whitening procedure) are compared.

Lastly, the condition indicator associated with the SGA-IPS (i.e. the proposed method without applying the whitening step) is presented in Figure 13(d). The condition indicator of the pinion does not change over measurement number and therefore it performs much better than the SA-IPS. Even though it is possible to see the two events in the condition indicator of the gear at measurement numbers 148 and 280, the condition indicator of the gear contains much more noise than the SA-IPS and SGA-GAW-IPS condition indicators shown in Figures 13(a) and 13(b). This specific noise is attributed to its sensitivity of the SGA-IPS to changes in operating conditions. Hence, by comparing the results in Figures 13(a) and 13(d), it is clear that the whitening procedure makes the condition indicator more sensitive to changes in machine condition and more robust to changes in operating condition.

Hence, the proposed method performs much better than the synchronous average of the instantaneous power spectrum, the synchronous average of the average whitened instantaneous power spectrum and the synchronous geometric averaged instantaneous power spectrum. This indicates that the combination of the proposed whitening procedure and the synchronous geometric average makes the method well-suited for applications under time-varying operating and impulsive noise conditions.

4. Conclusions

In this work, a new method is proposed to enhance the fault information in vibration signals. This method combines a synchronous geometric average whitening procedure with the synchronous geometric average of the whitened instantaneous power spectrum for fault diagnosis under time-varying operating conditions. It is shown on two experimental datasets that the proposed method is capable of attenuating the impulsive noise, while enhancing the damage under time-varying operating conditions.

Appendix A. Motivation behind method

It is assumed that the measured vibration signal

$$x(t) = x_c(t) + x_s(t), \tag{A.1}$$

can be decomposed in stationary $x_s(t)$ and cyclostationary parts $x_c(t)$. Furthermore, it is assumed that both parts can be decomposed in terms of a time-invariant impulse response function $h_i(t)$ and raw signal component $q_i(t)$ as follows:

$$x_i(t) = h_i(t) \otimes q_i(t). \tag{A.2}$$

The Instantaneous Power Spectrum (IPS) of the signal can therefore be written as follows:

$$I_{xx}(t,f) = |H_c(f)|^2 \cdot I_c(t,f) + |H_s(f)|^2 \cdot I_s(f), \tag{A.3}$$

where $I_c(t,f)$ is the IPS of the cyclostationary part and $I_s(f)$ is the spectrum of the stationary part. If the whitening function is defined as the PSD of the stationary part:

$$W(f) = |H_c(f)|^2 \cdot I_s(f), \tag{A.4}$$

then the whitened IPS would have the following form:

$$\frac{I_{xx}(t,f)}{W(f)} = \frac{|H_c(f)|^2}{|H_s(f)|^2} \cdot \frac{I_c(t,f)}{I_s(f)} + 1 \tag{A.5}$$

This whitened IPS would therefore enhance signals in frequency bands with low energy levels. If the whitening function is estimated with the time-average of the IPS

$$\hat{W}(f) = \left\langle I_{xx}(t,f) \right\rangle_t, \tag{A.6}$$

it is easy to show that Equation (A.3) can be written as

$$\hat{W}(f) = \left\langle |H_c(f)|^2 \cdot I_c(t,f) \right\rangle_t + W(f). \tag{A.7}$$

Hence, the average whitening function is dependent on the instantaneous power of the cyclostationary components $I_c(t,f)$. The instantaneous power spectrum is expected to increase as the machine degrades and therefore the whitening function would also change as the machine degrades. This means that the average whitening function would not be well-suited for applications where fault trending needs to be performed.

Appendix B. Synthetic signal

The synthetic signal is generated as follows:

$$x(t) = x_s(t) + x_c(t), \tag{B.1}$$

where x_s denotes the stationary components

$$x_s(t) = h_s(t) \cdot q_s(t) + \epsilon(t), \tag{B.2}$$

with $h_s(t)$ being the impulse response function of the stationary components, $q_s(t)$ is the raw signal component and $\epsilon(t)$ is white noise. The cyclostationary component is given by

$$x_c(t) = h_c(t) \cdot q_c(t, \mathrm{MF}), \tag{B.3}$$

where $h_c(t)$ is the corresponding impulse response function, $q_c(t, \mathrm{MF})$ is the raw signal component and MF is the Magnification Factor (MF) which is used to simulate a change in the condition of the machine.

The impulse response function of the stationary components $h_s(t)$ in Equation (B.2) is given by

$$\begin{aligned} h_s(t) =& e^{-50t} \sin(2 \cdot \pi \cdot 1000 \cdot t) + 0.2 \cdot e^{-100 \cdot t} \cdot \sin(2 \cdot \pi \cdot 2000 \cdot t) \\ &+ e^{-200 \cdot t} \cdot \sin(2 \cdot \pi \cdot 3500 \cdot t). \end{aligned} \tag{B.4}$$

The stationary signal in Equation (B.2) is generated by

$$q_s(t) \sim \mathcal{N}(0, 1^2), \tag{B.5}$$

which $\mathcal{N}(\mu, \sigma^2)$ denotes a Gaussian distribution with a mean of μ and a variance of σ^2. The white noise signal $\epsilon(t)$ in Equation (B.2) is given by

$$\epsilon(t) \sim \mathcal{N}(0, 1^2). \tag{B.6}$$

The CycloStationary (CS) part of the synthetic signal given by Equation (B.3), simulates the presence of damage. The impulse response function of the CS components is given by

$$h_c(t) = e^{-100 \cdot t} \cdot \sin(2 \cdot \pi \cdot 2000 \cdot t). \tag{B.7}$$

The raw CS signal, given by

$$q_c(t, \mathrm{MF}) = \sum_{k=0}^{N_c - 1} A_k(\mathrm{MF}) \cdot \delta\left(t - k \cdot 1\right), \tag{B.8}$$

consists of a train of N_c Dirac functions $\delta(\cdot)$, spaced with a period of 1 second. The amplitude of the kth impulse is generated by

$$A_k(\mathrm{MF}) = \begin{cases} a_k \sim \mathcal{N}(\mathrm{MF}, 0.2^2) & \text{if MF} \geq 10 \\ 0 & \text{if MF} = 0 \end{cases}. \tag{B.9}$$

Hence, as the Magnification Factor (MF) increase, the magnitude of the CS increases as well.

In Figure B.14(a), the PSD of the stationary part is compared to the PSD of the CS part for different Magnification Factors (MF). The purpose of the whitening procedure is to attenuate the stationary components, while being insensitive to changes in the CS components. The Average Whitening (AW) and the Geometric Average Whitening (GAW) functions, denoted here by

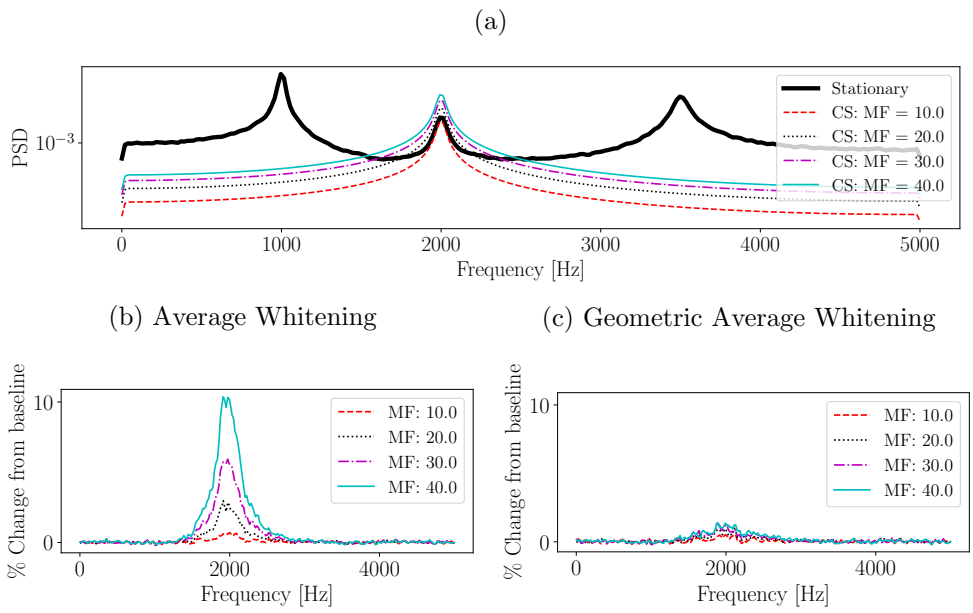

Figure B.14: The Power Spectral Densities (PSD) of the different components in Equation (B.1) are shown in Figure B.14(a), with the sensitivity of the whitening function to different Magnification Factors (MF) shown in Figures B.14(b) and B.14(c).

$W_{AW}(f)$ and $W_{GAW}(f)$, are calculated for the synthetic signal with different magnification factors. The change from the baseline of the ith whitening function $W_i(f)$

$$\%\text{change from baseline} = \left| \frac{W_i(f) - W_i^0(f)}{W_i^0(f)} \right|, \tag{B.10}$$

is used to quantify the robustness of the ith whitening method. The baseline function $W_i^0(f)$ is defined by the whitening function calculated for the signal with MF = 0. The change from baseline is shown in Figures B.14(b) and B.14(c) for the two whitening functions. Since the stationary part remains the same, the whitening function should not change as the MF increases. The results in Figures B.14(b) and B.14(c) indicate that the GAW function is much more robust to changes in the MF than the AW and would therefore be more appropriate to attenuate the stationary components without attenuating the fault information. Hence, the GAW function should be preferred to the AW function.

Acknowledgements

The Eskom Power Plant Engineering Institute (EPPEI) is gratefully acknowledged for their support in the execution of this research.

References

[1] R. B. Randall, J. Antoni, Rolling element bearing diagnostics - A tutorial, Mechanical Systems and Signal Processing 25 (2) (2011) 485–520.

[2] J. P. Salameh, S. Cauet, E. Etien, A. Sakout, L. Rambault, Gearbox condition monitoring in wind turbines: A review, Mechanical Systems and Signal Processing 111 (2018) 251–264.

[3] T. Wang, Q. Han, F. Chu, Z. Feng, Vibration based condition monitoring and fault diagnosis of wind turbine planetary gearbox: A review, Mechanical Systems and Signal Processing 126 (2019) 662–685.

[4] J. Antoni, The infogram: Entropic evidence of the signature of repetitive transients, Mechanical Systems and Signal Processing 74 (2016) 73–94.

[5] D. Wang, X. Zhao, L.-L. Kou, Y. Qin, Y. Zhao, K.-L. Tsui, A simple and fast guideline for generating enhanced/squared envelope spectra from spectral coherence for bearing fault diagnosis, Mechanical Systems and Signal Processing 122 (2019) 754–768.

[6] J. Antoni, Cyclostationarity by examples, Mechanical Systems and Signal Processing 23 (4) (2009) 987–1036.

[7] A. Mauricio, W. A. Smith, R. B. Randall, J. Antoni, K. Gryllias, Improved envelope spectrum via feature optimisation-gram (iesfogram): A novel tool for rolling element bearing diagnostics under non-stationary operating conditions, Mechanical Systems and Signal Processing 144 (2020) 106891.

[8] R. Zimroz, W. Bartelmus, T. Barszcz, J. Urbanek, Diagnostics of bearings in presence of strong operating conditions non-stationarity - A procedure of load-dependent features processing with application to wind turbine bearings, Mechanical Systems and Signal Processing 46 (1) (2014) 16–27.

[9] S. Schmidt, P. S. Heyns, Normalisation of the amplitude modulation caused by time-varying operating conditions for condition monitoring, Measurement 149 (2020) 106964.

[10] W. Bartelmus, R. Zimroz, A new feature for monitoring the condition of gearboxes in non-stationary operating conditions, Mechanical Systems and Signal Processing 23 (5) (2009) 1528–1534.

[11] X. Xu, M. Zhao, J. Lin, Y. Lei, Envelope harmonic-to-noise ratio for periodic impulses detection and its application to bearing diagnosis, Measurement 91 (2016) 385–397.

[12] J. Antoni, Fast computation of the kurtogram for the detection of transient faults, Mechanical Systems and Signal Processing 21 (1) (2007) 108–124.

[13] J. Hebda-Sobkowicz, R. Zimroz, A. Wyłomańska, Selection of the informative frequency band in a bearing fault diagnosis in the presence of non-gaussian noisecomparison of recently developed methods, Applied Sciences 10 (8) (2020) 2657.

[14] J. Hebda-Sobkowicz, R. Zimroz, M. Pitera, A. Wyłomańska, Informative frequency band selection in the presence of non-gaussian noise–a novel approach based on the conditional variance statistic with application to bearing fault diagnosis, Mechanical Systems and Signal Processing 145 (2020) 106971.

[15] T. Wang, Q. Han, F. Chu, Z. Feng, A new skrgram based demodulation technique for planet bearing fault detection, Journal of Sound and Vibration 385 (2016) 330–349.

[16] Y. Miao, M. Zhao, J. Lin, Periodicity-impulsiveness spectrum based on singular value negentropy and its application for identification of optimal frequency band, IEEE Transactions on Industrial Electronics 66 (4) (2018) 3127–3138.

[17] J. Antoni, R. B. Randall, The spectral kurtosis: Application to the vibratory surveillance and diagnostics of rotating machines, Mechanical Systems and Signal Processing 20 (2) (2006) 308–331.

[18] W. A. Smith, P. Borghesani, Q. Ni, K. Wang, Z. Peng, Optimal demodulation-band selection for envelope-based diagnostics: A comparative study of traditional and novel tools, Mechanical Systems and Signal Processing 134 (2019) 106303.

[19] C. Peeters, J. Antoni, J. Helsen, Blind filters based on envelope spectrum sparsity indicators for bearing and gear vibration-based condition monitoring, Mechanical Systems and Signal Processing 138 (2020) 106556.

[20] J. Wodecki, A. Michalak, R. Zimroz, Optimal filter design with progressive genetic algorithm for local damage detection in rolling bearings, Mechanical Systems and Signal Processing 102 (2018) 102–116.

[21] D. Wang, An extension of the infograms to novel bayesian inference for bearing fault feature identification, Mechanical Systems and Signal Processing 80 (2016) 19–30.

[22] X. Xu, Z. Qiao, Y. Lei, Repetitive transient extraction for machinery fault diagnosis using multiscale fractional order entropy infogram, Mechanical Systems and Signal Processing 103 (2018) 312–326.

[23] S. Schmidt, A. Mauricio, P. S. Heyns, K. C. Gryllias, A methodology for identifying information rich frequency bands for diagnostics of mechanical components-of-interest under time-varying operating conditions, Mechanical Systems and Signal Processing 142 (2020) 106739.

[24] Z. Liu, Y. Jin, M. J. Zuo, D. Peng, Accugram: A novel approach based on classification to frequency band selection for rotating machinery fault diagnosis, ISA transactions 95 (2019) 346–357.

[25] D. Abboud, J. Antoni, S. Sieg-Zieba, M. Eltabach, Envelope analysis of rotating machine vibrations in variable speed conditions: A comprehensive treatment, Mechanical Systems and Signal Processing 84 (2017) 200–226.

[26] S. Schmidt, P. S. Heyns, J. P. de Villiers, A novelty detection diagnostic methodology for gearboxes operating under fluctuating operating conditions using probabilistic techniques, Mechanical Systems and Signal Processing 100 (2018) 152–166.

[27] R. B. Randall, A history of cepstrum analysis and its application to mechanical problems, Mechanical Systems and Signal Processing 97 (2017) 3–19.

[28] P. Borghesani, P. Pennacchi, R. Randall, N. Sawalhi, R. Ricci, Application of cepstrum prewhitening for the diagnosis of bearing faults under variable speed conditions, Mechanical Systems and Signal Processing 36 (2) (2013) 370–384.

[29] D. Abboud, J. Antoni, S. Sieg-Zieba, M. Eltabach, Deterministic-random separation in nonstationary regime, Journal of Sound and Vibration 362 (2016) 305–326.

[30] J. Obuchowski, A. Wylomanska, R. Zimroz, Selection of informative frequency band in local damage detection in rotating machinery, Mechanical Systems and Signal Processing 48 (1-2) (2014) 138–152.

[31] J. Sokołowski, J. Obuchowski, A. Wyłomańska, P. Kruczek, R. Zimroz, Multiple local damage detection method based on time-frequency representation and agglomerative hierarchical clustering of temporary spectral content, Applied Acoustics 147 (2019) 44–55.

[32] Z. Feng, M. Liang, F. Chu, Recent advances in time–frequency analysis methods for machinery fault diagnosis: A review with application examples, Mechanical Systems and Signal Processing 38 (1) (2013) 165–205.

[33] L. Wang, Z. Liu, Q. Miao, X. Zhang, Time–frequency analysis based on ensemble local mean decomposition and fast kurtogram for rotating machinery fault diagnosis, Mechanical Systems and Signal Processing 103 (2018) 60–75.

[34] Z. Feng, X. Yu, D. Zhang, M. Liang, Generalized adaptive mode decomposition for non-stationary signal analysis of rotating machinery: Principle and applications, Mechanical Systems and Signal Processing 136 (2020) 106530.

[35] N. Baydar, A. Ball, Detection of gear deterioration under varying load conditions by using the instantaneous power spectrum, Mechanical Systems and Signal Processing 14 (6) (2000) 907–921. doi:10.1006/mssp.1999.1281.

[36] J. Urbanek, T. Barszcz, R. Zimroz, J. Antoni, Application of averaged instantaneous power spectrum for diagnostics of machinery operating under non-stationary operational conditions, Measurement 45 (7) (2012) 1782–1791.

[37] J. Antoni, D. Hanson, Detection of Surface Ships From Interception of Cyclostationary Signature With the Cyclic Modulation Coherence, IEEE Journal of Oceanic Engineering 37 (3) (2012) 478–493.

[38] D. Abboud, J. Antoni, Order-frequency analysis of machine signals, Mechanical Systems and Signal Processing 87 (October 2016) (2017) 229–258.

[39] D. Abboud, J. Antoni, M. Eltabach, S. Sieg-Zieba, Angle\time cyclostationarity for the analysis of rolling element bearing vibrations, Measurement 75 (2015) 29–39.

[40] C. Peeters, Q. Leclère, J. Antoni, P. Lindahl, J. Donnal, S. Leeb, J. Helsen, Review and comparison of tacholess instantaneous speed estimation methods on experimental vibration data, Mechanical Systems and Signal Processing 129 (2019) 407–436.

[41] S. Lu, R. Yan, Y. Liu, Q. Wang, Tacholess speed estimation in order tracking: A review with application to rotating machine fault diagnosis, IEEE Transactions on Instrumentation and Measurement 68 (7) (2019) 2315–2332.

[42] J. Antoni, Cyclic spectral analysis of rolling-element bearing signals: Facts and fictions, Journal of Sound and Vibration 304 (3-5) (2007) 497–529.

[43] A. Wyłomańska, G. Żak, P. Kruczek, R. Zimroz, Application of tempered stable distribution for selection of optimal frequency band in gearbox local damage detection, Applied Acoustics 128 (2017) 14–22.

[44] J. Wodecki, P. Kruczek, A. Bartkowiak, R. Zimroz, A. Wyłomańska, Novel method of informative frequency band selection for vibration signal using nonnegative matrix factorization of spectrogram matrix, Mechanical Systems and Signal Processing 130 (2019) 585–596.

[45] J. Antoni, P. Borghesani, A statistical methodology for the design of condition indicators, Mechanical Systems and Signal Processing 114 (2019) 290–327.

[46] G. L. McDonald, Q. Zhao, M. J. Zuo, Maximum correlated kurtosis deconvolution and application on gear tooth chip fault detection, Mechanical Systems and Signal Processing 33 (2012) 237–255.

[47] Y. Miao, M. Zhao, J. Lin, Y. Lei, Application of an improved maximum correlated kurtosis deconvolution method for fault diagnosis of rolling element bearings, Mechanical Systems and Signal Processing 92 (2017) 173–195.

[48] Y. Lei, N. Li, L. Guo, N. Li, T. Yan, J. Lin, Machinery health prognostics: A systematic review from data acquisition to RUL prediction, Mechanical Systems and Signal Processing 104 (2018) 799–834.

[49] A. Raad, J. Antoni, M. Sidahmed, Indicators of cyclostationarity: Theory and application to gear fault monitoring, Mechanical Systems and Signal Processing 22 (3) (2008) 574–587.

[50] C. Hu, W. A. Smith, R. B. Randall, Z. Peng, Development of a gear vibration indicator and its application in gear wear monitoring, Mechanical Systems and Signal Processing 76-77 (2016) 319–336.